Gui Yang,[1] Xianhong Hu,[2] Qian Feng,[2] and Sanjay Nimbalkar[3]

Laboratory and Constitutive Modeling of Critical State Behavior of Rockfill Aggregates Mixed with Polymer

Reference

[1] Key Laboratory of Ministry of Education for Geomechanics and Embankment Engineering, College of Civil and Transportation Engineering, Hohai University, 1 Xikang Rd., Nanjing 210098, People's Republic of China (Corresponding author), e-mail: ygheitu@163.com, https://orcid.org/0000-0002-2611-7464

[2] Key Laboratory of Ministry of Education for Geomechanics and Embankment Engineering, College of Civil and Transportation Engineering, Hohai University, 1 Xikang Rd., Nanjing 210098, People's Republic of China

[3] School of Civil and Environmental Engineering, Faculty of Engineering and Information Technology, University of Technology Sydney, City Campus, PO Box 123 Broadway, New South Wales 2007, Australia

ABSTRACT

In order to increase the strength and deformation properties of coarse aggregates, the polymer was used as an additive. In this study, a series of triaxial tests were performed to analysis the effect of polymer content on the strength, deformation, and critical state of rockfill aggregates. It is found that the deformation properties are the same for different polymer contents. As the polymer content increases, the peak stress increases, and the volume strain decreases. The addition of polymer mainly led to inducing cohesion in rockfill aggregates while showing a marginal influence on friction angle. The average effective stress, which considered the cohesion of polymer as additional effective stress, was modified. It was observed that the critical state envelopes in q–p'_{pc} and e–p'_{pc} were not much influenced by the addition of polymer. A state parameter is used as a function of void ratio and pressure. A boundary surface model of polymer rockfill aggregates based on the critical state approach was proposed. The performance of the model is demonstrated by the results of triaxial tests. The study shows the model could effectively capture the influence of polymer contents and confining pressures on strength and deformation characteristics of rockfill aggregates.

Keywords

polymer, critical state, monotonic loads, cohesion, constitutive relations

Introduction

The reinforced soil has been widely used as it can significantly improve the strength of the soil and reduce the deformation. Depending upon the form of reinforcement, it can be divided into two types: (1) planar reinforcement and (2) 3-D reinforcement. In the first type, the reinforced material and the soil are in planar contact and are arranged in layers,

such as geogrid and geotextile.[1–4] The reinforced soil obeys the Mohr–Coulomb strength failure criterion, and the friction angle remains unchanged or slightly improved after the geogrid installation. The effect of reinforcement is mainly reflected in the quasicohesion of the soil. The reinforcement mechanism can be explained by the concept of equivalent confining pressure.[5,6] The reinforcement effect increases as the axial deformation increases.

The other type is 3-D reinforcement, which provides better contact between the reinforced material and the soil. It is either arranged in layers or evenly distributed in the soil. This type can be divided into two categories: (1) distributed fibers or blended cementitious agents and (2) cellular material derived from polymer fiber, glass fiber, and geocell.[7–11] The strength of the reinforced soil is related to the content, shape, and size of the reinforced material. The effect of fiber reinforcement is mainly reflected in the friction angle, which has little effect on the cohesion. The other type is binding materials such as cement, fly ash, polyurethane chemical grouting materials, etc.[12–16] These materials bind the soil particles together to increase the cohesion, thereby improving the shear strength, improving the deformation characteristics, and resisting liquefaction characteristics. In the case of low content of cementitious materials, the static mechanical properties of cementitious or fly ash materials are similar to those of soil. After reinforcement, the friction angle of soil remains almost constant, whereas the cohesion and shear modulus show substantial change. The bonding effect is related to factors such as cement dosage, water-cement ratio, pore-to-cement volume ratio, particle shape, particle arrangement, and sample density. Compared with fiber reinforcement, cement reinforcement induces brittle failure in soils. Fiber reinforcement has no obvious influence on the initial elastic modulus of the soil, and cement reinforcement significantly improves the initial elastic modulus of the soil.[17]

With the development of science and technology, chemical grouting technology has been widely used in engineering projects. At present, such technologies are mostly used for seepage prevention and foundation reinforcement of dam and levee works. Common grouting materials are cement, clay, polyurethane, and epoxy. Among them, polyurethanes are widely used in engineering. Owing to the convenience and high shear strength, rockfill have been widely used in hydraulic engineering, civil engineering, and transport engineering, among others[18–20] The strength and deformation properties have also been studied. In some special cases, polymer are injected into the rockfill to improve the strength and settlement deformation of rockfill[21–23] The mixture of polymer and rockfill is called polymer rockill, and it can effectively reduce its long-term deformation and reduce it by more than 70%.[24,25]

Duncan Model is a typical nonlinear model, which has been widely used for simulating rockfill because of its simple formula and easy parameter acquisition.[26] However, the model cannot reflect the anisotropic and dilatancy properties, and the model based on the theory of elasticity can make up for this shortcoming, such as Pastor-Zienkiewicz model.[27] However, when the model considers the pressure correlation, its parameters are influenced by the average main stress, and there are some limitations in the application of high earth and stone dam static and dynamic analysis. Some constitutive model[28–30] considering the state concept and particle breakage have been proposed. Another model with more research is one based on boundary surface theory. The model has great advantages in describing the nonproportional loading and antho-heterogeneousness of soil. The model allows plastic deformation within the boundary surface, avoids the mutation from the elastic state to the plastic state, and can better describe the stress response within the boundary surface.[31–33]

In this paper, rockfill aggregates mixed with polymer are proposed for the seismic strengthening of high earth-rock dams. A series of laboratory tests using triaxial apparatus are carried out to study the strength and deformation characteristics of polymeric rockfill under different polymer contents. The constitutive relations with reference to bounding surface and critical state behavior are also discussed.

Laboratory Testing

The triaxial apparatus, which can accommodate a rockfill specimen with 100 mm in diameter and 200 mm in height, was used. The maximum cell pressure is 1 MPa, and the maximum axial loading capacity is 60 kN. The coarse-grained material was collected from a quarry in Nanjing, China. The grain size distributions of

FIG. 1   Grain size distribution and triaxial apparatus for tests. (*A*) Grading curve and (*B*) triaxial apparatus.
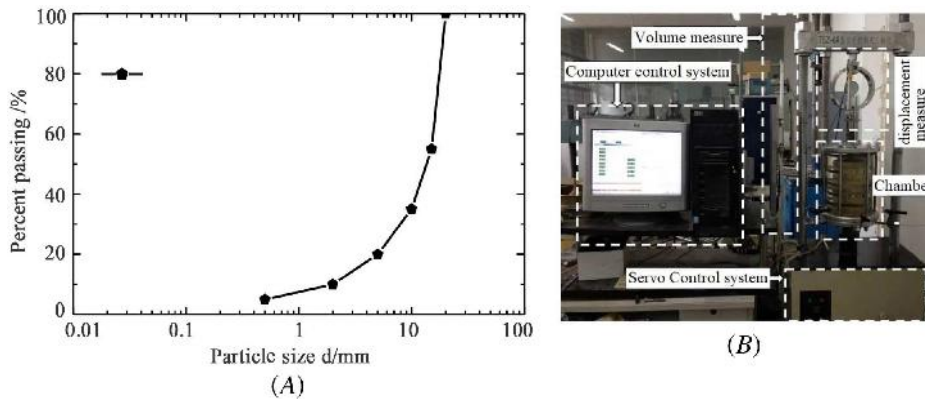
the material and triaxial apparatus are shown in **figure 1**. Based on values of coefficient of uniformity and coefficient of curvature ($C_u = 11.5$, $C_c = 2.98$), the rockfill was classified as well-graded material. The density is 1.81 g/cm^3, which is relevant to placement density in the field.

The polymer material used in the test was a binary mix of polyurethane foaming agents with mix proportion of 1:1. These agents are categorized into Class A and Class B materials. The Class A material is a dark brown transparent liquid with isocyanate composition. The density is 1.2 g/cm^3. The Class B material is a yellow transparent liquid composed of a combined polyether. Its viscosity is higher than Class A material. The density is 1.1 g/cm^3. Both A and B materials are stirred and mixed to prepare uniformly blended mix with the ratio of 1:1. In order to measure the influence of polymer material on the mechanical properties of coarse material, the polymer content R_p is defined as follows:

$$R_p = \frac{M_p}{M_R}$$

(1)

where M_p and M_R are the masses of polymer and coarse aggregates, respectively.

The polymer and rockfill material were divided into five portions. Each polymer Class A and B portion are mixed first, then mixed with each rockfill portion, and finally poured into the split cylindrical mold for compaction to the preset height. The mix was then compacted to the preset height. The prepared test specimens at varying polymer content R_P of 0–4 % are shown in **figure 2**. The specimen ($R_P = 2$ and 4 %) was saturated by

FIG. 2

Test specimen showing a range of polymeric rockfill aggregates.

vacuum, with a negative pressure of 0.1 MPa and pumping time of 1 h. Then, the sample was placed inside test chamber. The specimen ($R_P = 0$ %) was directly placed inside test chamber. Before commencement of monotonic shear test, the sample was saturated by allowing water to pass through the base of the triaxial cell under a back pressure of 10 kPa. The monotonic shearing rate of displacement was determined to be 0.6 mm/min.[34] Four different values of external confining pressures were selected (i.e., $\sigma'_3 = 0.3$, 0.5, 0.7 and 0.9 MPa) in order to resemble the in situ stresses.

Results Analysis

STRESS–STRAIN AND VOLUME CHANGE RESPONSE

The stress–strain and volume change behavior of rockfill aggregates at different polymer content Rp of 0 %, 2 % and 4 % are shown in **figures 3–5**, respectively. It is evident that the deviatoric stress–axial strain relationship is nonlinear. The strain-softening is not obvious at low confining pressure. As the strain increases, the stress eventually tends to a stable value. From the volume strain–axial strain relationship, it can be seen that the sample is generally compressed with no sign of substantial dilation. As the monotonic shearing is continued until the axial strain reaches about 25%, the deviatoric stress and the volume strain exhibit a stable value, indicating the critical state. As the polymer content increases, the peak stress increases, the volume strain decreases, and the strain to reach the critical state increases. This is because of the polymer fills the voids of the rockfill and participate in the stress transfer across interparticular contacts. The bonding force between the rockfill increases during the loading process compared with rockfill without polymer. Subsequently, the deviatoric strength increases, and the volumetric strain decreases.

Figure 6 shows the test results for rockfill aggregates mixed at different polymer contents within the given range of confining pressures ($\sigma'_3 = 0.3$–0.9 MPa). It can be seen that the deviator stress increases with the increase of the polymer content and the influence of the polymer content in the low strain region is greater. As the axial strain increases, the influence of polymer additive seems to gradually decrease. The main reason is that with the increase of axial strain, the deformation between particles increases. The bonding force caused by polymer is

FIG. 3

Stress–strain volume behavior of rockfill aggregates without polymer ($R_p = 0$ %).
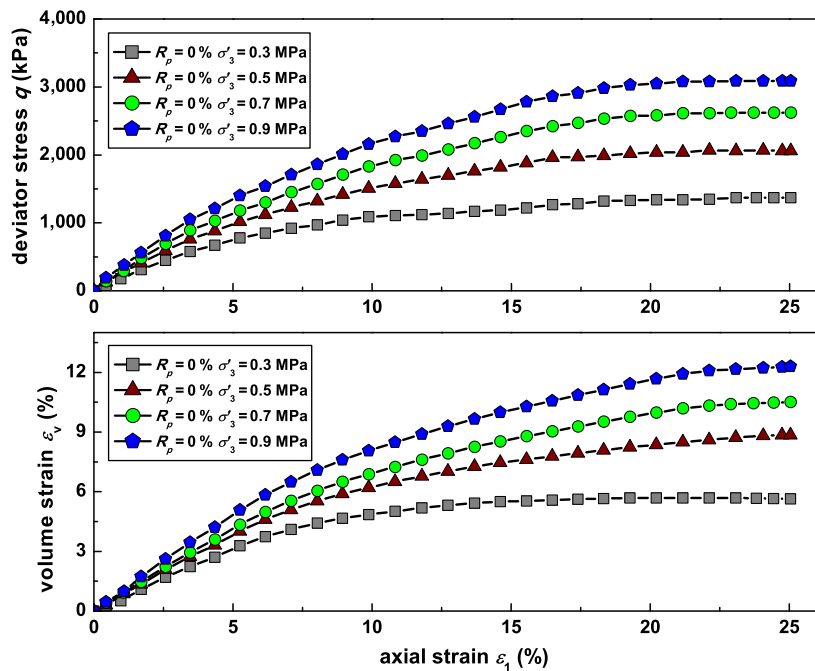
FIG. 4

Stress–strain volume behavior of rockfill aggregates with polymer ($R_p = 2$ %).
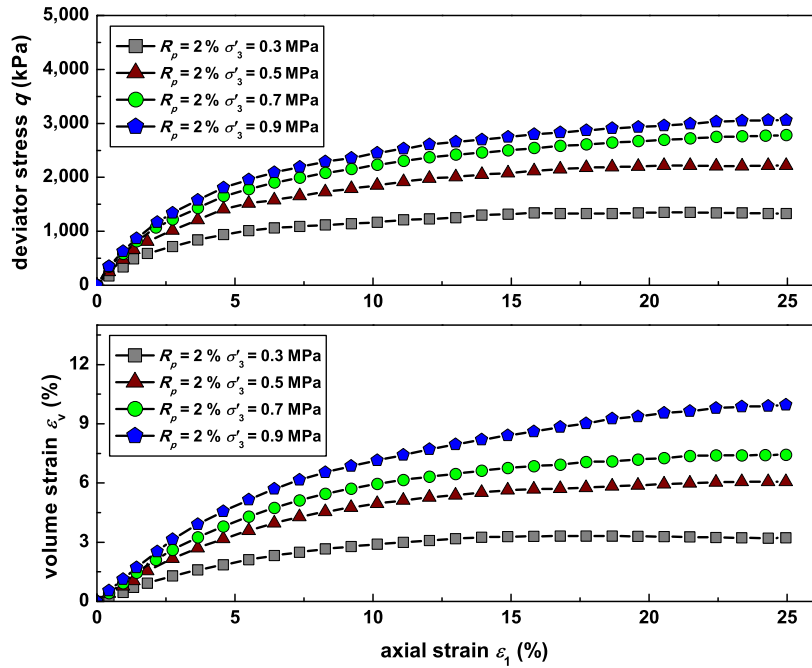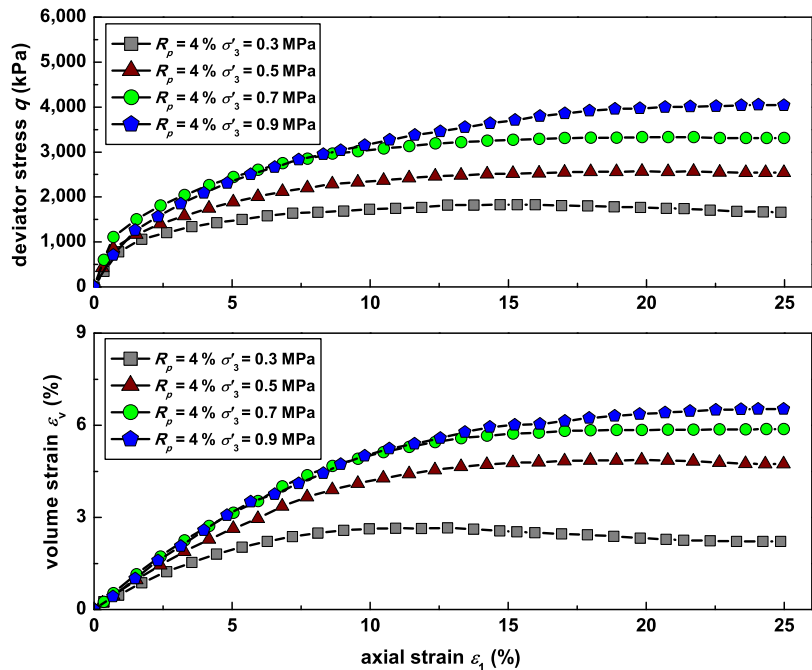

FIG. 5

Stress–strain volume behavior of rockfill aggregates with polymer ($R_p = 4$ %).

gradually destroyed. After the bonding force is destroyed, the action of the polymer affects the friction coefficient between the particles. Because of the low content of polymer, its influence on the friction coefficient is also small. The residual strength of rockfill with polymer content of 2 % is almost equal to the residual strength of rockfill

FIG. 6

Stress–strain volume
behavior of rockfill
aggregates with
different polymer R_p.
(*A*) Confining pressure
$\sigma'_3 = 0.3$ MPa and
(*B*) $\sigma'_3 = 0.9$ MPa.
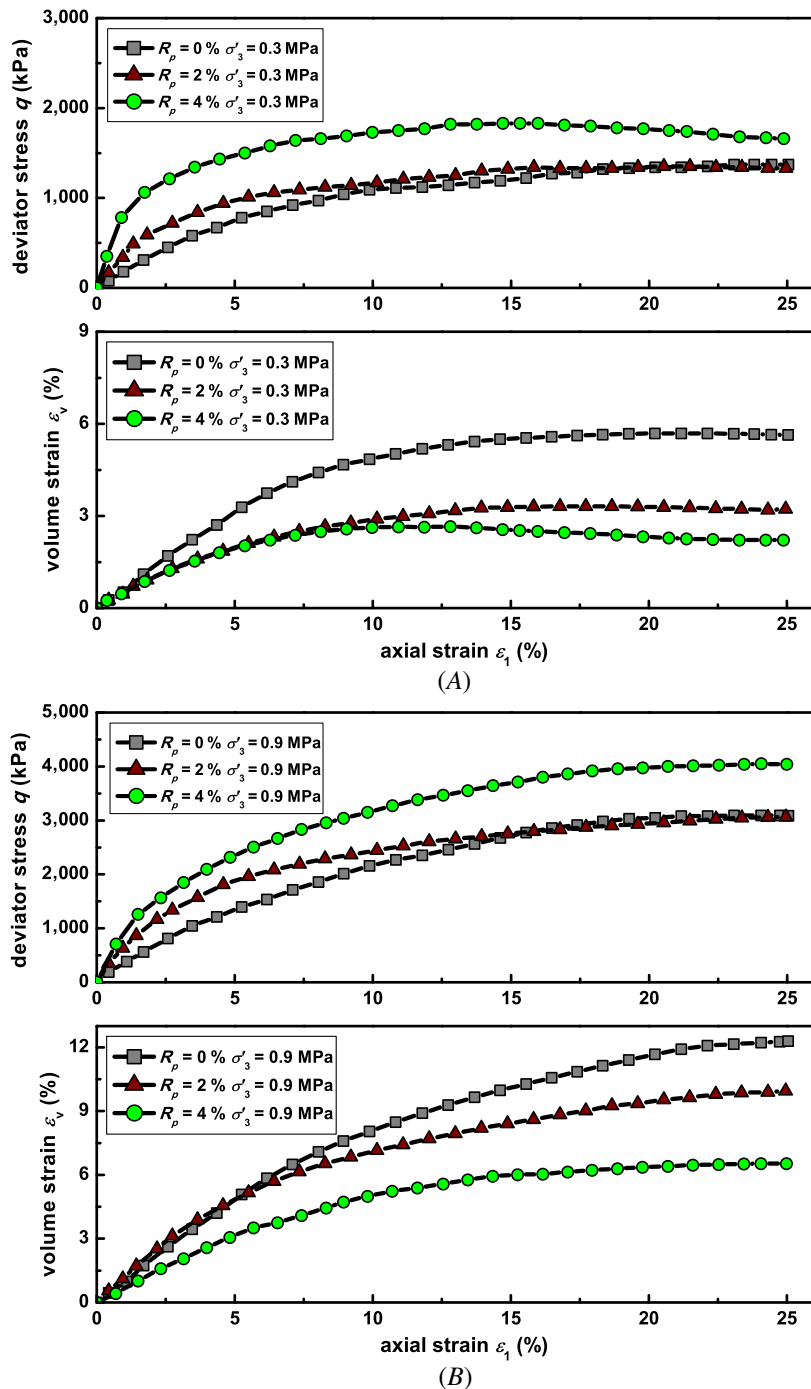
without the addition of polymer, i.e., $R_p = 0$ %. This is mainly due to the fact that adhesion between the particles at the lower strain can play a greater role in strength, but when the axial strain is very large, the adhesion between the particles is destroyed. The volumetric strain decreases with the increase of polymer content. The difference of volumetric strain of polymeric rockfill between $R_p = 2$ % and $R_p = 4$ % at low confining pressure is small, and the

difference increases with the increase of axial strain. At larger confining pressure, the difference in volumetric strain between polymer content 0 % and 2 % is small, and the difference gradually increases with the increase of axial strain and eventually approaches a stable value.

CRITICAL STATE LINE IN q-p'

In order to capture the effect of adhesive polymer, the concept of modified average stress is used, which considers the effects of cohesion and friction angle. The modified average effective stress p'_{pc} is expressed as follows:

$$p'_{pc} = p' + c'/\tan(\varphi')$$

(2)

where p' is the average effective stress (kPa), c' is effective cohesion (kPa), and φ' is the frictional angle (degree) defined as follows:

$$\varphi' = \varphi'_0 - \Delta\varphi' \log(p'/p_a)$$

(3)

where φ'_0 is the initial effective frictional angle (degree), $\Delta\varphi'$ is the increment of internal frictional angle (degree), and $p_a = 101$ kPa is the atmospheric pressure used for the purpose of normalization.

The polymer effect can be called additional average effective stress ($\Delta p' = c'/\tan(\varphi')$). The strength parameters of coarse rockfill aggregates mixed with and without polymer are listed in Table 1. It is evident that the polymer content mainly influences the cohesion. The values of frictional angle are less affected by polymer content.

The critical state lines of the aggregates-polymer mix are plotted in the p'_{pc}–q plane as shown in figure 7, and a linear equation can be used to illustrate the evolution trend. It is apparent that the critical stress ratio ($M_{cs} = q/p'_{pc} = 1.66$) is constant for different content of polymer rockfill.

TABLE 1

Strength parameters of polymeric material

R_p	c', kPa	φ'_0, °	$\Delta\varphi'$, °
0 %	0	49	10.1
2 %	70	49.4	10.7
4 %	113	50.6	10.6

FIG. 7

Critical state line in q–p'_{pc} plane of different contents of coarse polymer.
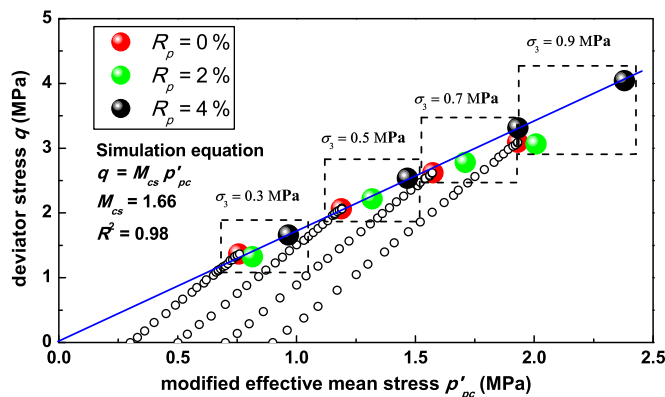
CRITICAL STATE LINE IN $e\text{–}p'$

Because of the significant particle breakage under high stresses, the critical state line of $e\text{–}p'$ no longer remains a straight line but presents a nonlinearity corresponding to the increase in confining pressure. In tests, the polymer content is very small, which cannot completely fill the pores between the particles. The initial void ratio e_0 is calculated as follows:

$$e_0 = \frac{V_v}{V_s} \tag{4}$$

where V_v is the volume of voids, and V_s is the volume of solids.

The polymer can be considered either as voids or as solids. When the polymer is considered as solids, the total volume of solids V_s is the sum of rockfill aggregates V_{sr} and polymer V_{sp}. The volume of the polymer V_{sp} is calculated according to the polymer content ($V_{sp} = m_p/\rho_{avp}$, where m_p is the mass of polymer in the sample and ρ_{avp} is the average density of polymer). Therefore, two types of critical state void ratio can be defined. The critical state envelopes of polymeric rockfill are plotted in the $e\text{–}(p'_{pc}/p_a)^{0.7}$ plane as shown in **figure 8**. It has been shown that there is a good linear relationship. The expression is given by Li and Wang[35] as follows:

$$e_{cs} = e_{cs0} - \lambda_s \left(\frac{p'_{pc}}{p_a}\right)^{\xi} \tag{5}$$

where e_{cs} denotes the critical state void ratio, and e_{cs0} and λ_s are dimensionless material constants. The parameter $\xi = 0.7$ is used in this study, which shows good resemblance to the laboratory data.

According to **figure 8A**, the critical state lines of different polymer contents are parallel to each other, and their intercepts e_{cs0} increase as the polymer content increases. However, when the polymer is considered as solids, the content polymer has little influence on the critical state line, as shown in **figure 8B**.

FIG. 8

Critical state line in the $e\text{–}(p'_{pc}/p_a)^{0.7}$ plane for polymer rockfill. (*A*) Polymer considered as voids and (*B*) polymer considered as solids.
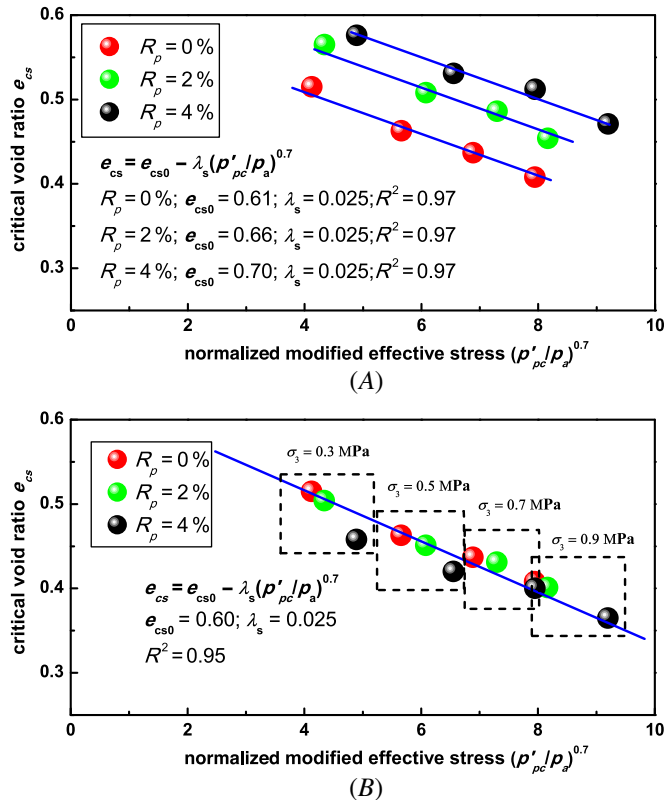
Bounding Surface Plastic Model

Many state indexes are proposed, such as void ratio state parameter and pressure index.[36,37] The state parameter I_{ep} proposed by Xiao and Liu[30] is adopted for consideration of the particle breakage characteristics of rockfill. The expression is as follows:

$$I_{ep} = \frac{e}{e_{cs}} \frac{p'_{pc}}{p'_{cs}} \tag{6}$$

where $p'_{cs} = p_a \left(\frac{e_{cs}-e}{\lambda_s}\right)^{1/0.7}$. The elastic shear modulus G is correlated with the void ratio and stress state, which can be expressed as follows:

$$G = G_0 \frac{(2.97-e)^2}{1+e} \sqrt{\frac{p'_{pc}}{p_a}} \tag{7}$$

where G_0 is the material constant, and e is the current void ratio. The loading surface takes the following form[38]:

$$f(p'_{pc}, q, p_c) = \left(\frac{q}{M_{cs}p'_{pc}}\right)^N - \frac{\ln(p_c/p'_{pc})}{\ln R} = 0 \tag{8}$$

where p_c is an isotropic hardening parameter, q is deviatoric stress, and R and N are material constants, respectively.

The unit normal vector at the image point defining the direction of loading is defined as follows:

$$n_v^f = \left(-\frac{q}{p'_{pc}}\left(1-1/N \times \ln\left(\frac{p_c}{p'_{pc}}\right)\right)\right) \Big/ \sqrt{\left(-\frac{q}{p'_{pc}}\left(1-1/N \times \ln\left(\frac{p_c}{p'_{pc}}\right)\right)\right)^2 + 1} \tag{9}$$

$$n_s^f = 1 \Big/ \sqrt{\left(-\frac{q}{p'_{pc}}\left(1-1/N \times \ln\left(\frac{p_c}{p'_{pc}}\right)\right)\right)^2 + 1} \tag{10}$$

The plastic potential defines the ratio between the incremental plastic volumetric strain and plastic shear strain. The form used here is

$$d = (M_d^2 - \eta^2)/2\eta \tag{11}$$

where d is dilatancy; $M_d = M_{cs}(1+k_d\log(I_{ep}))$; and $\eta = q/p'_{pc}$ is the stress ratio. The unit vector of plastic flow is defined as follows:

$$n_v^g = \frac{(M_d^2 - \eta^2)/2\eta}{\sqrt{1 + ((M_d^2 - \eta^2)/2\eta)^2}} \tag{12}$$

$$n_s^g = \frac{1}{\sqrt{1 + ((M_d^2 - \eta^2)/2\eta)^2}} \tag{13}$$

The plastic modulus H_p is defined as follows[39]:

$$H_p = (h_1 - h_2 e_0)\left(1 - \frac{I_{ep}}{2}\right) G \frac{M_b - \eta}{\eta} \frac{1}{(1+\eta)^2} \tag{14}$$

where h_1 and h_2 are material constants, respectively; $M_b = M_{cs}(1+k_b\log(I_{ep}))$; and e_0 is the initial void ratio.

Based on the assumption of the nonassociated flow rule, the increments of elastic and plastic strain in the bounding plasticity theory can be expressed as follows:

FIG. 9

Test and computed results of polymer rockfill. (*A*) Confining pressure $\sigma'_3 = 0.5$ MPa and (*B*) $\sigma'_3 = 0.9$ MPa.
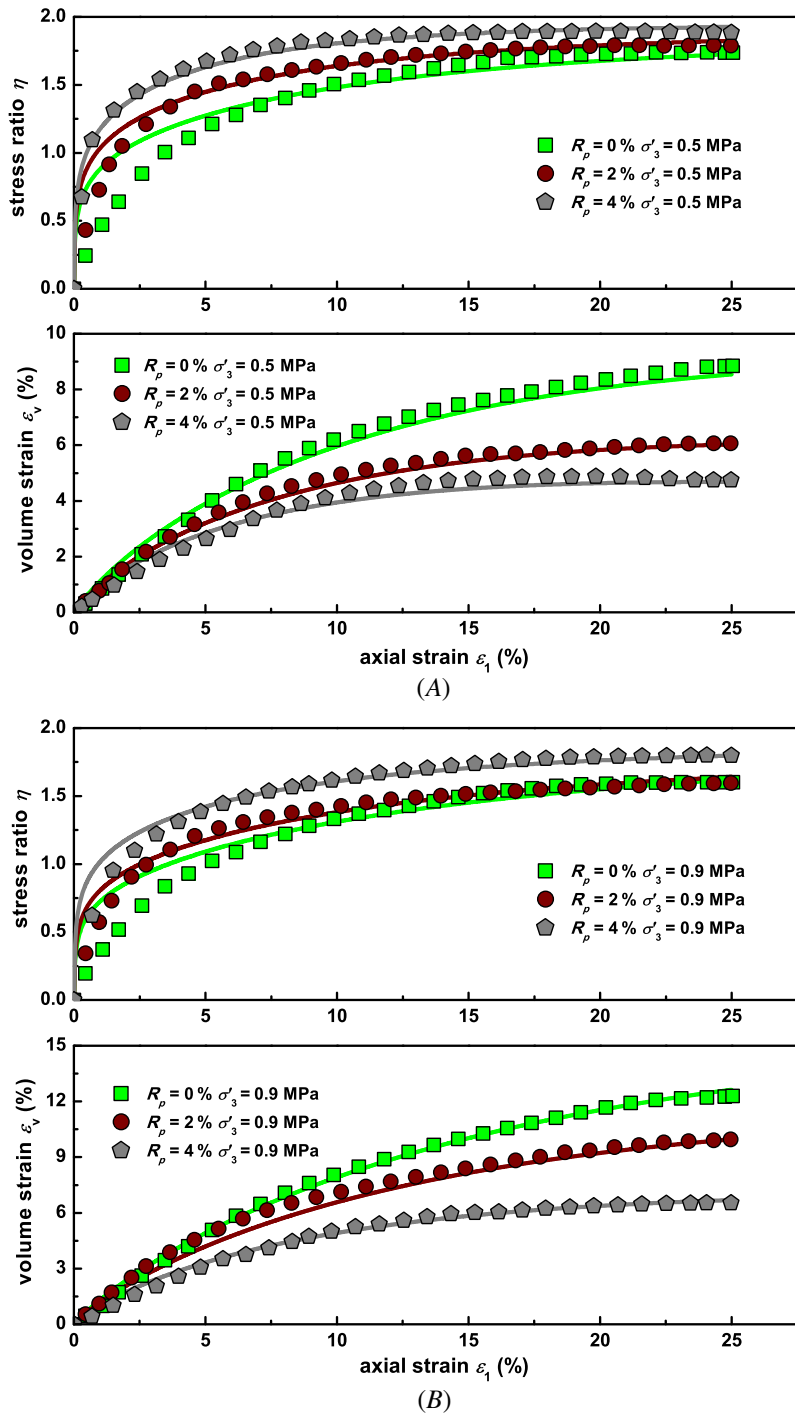
$$\begin{cases} d\varepsilon_v = d\varepsilon_v^e + d\varepsilon_v^p = \dfrac{dp'_{pc}}{B} + \dfrac{(n_v^f dp'_{pc} + n_s^f dq)n_v^g}{H_p} \\ d\varepsilon_s = d\varepsilon_s^e + d\varepsilon_s^p = \dfrac{dq}{3G} + \dfrac{(n_v^f dp'_{pc} + n_s^f dq)n_s^g}{H_p} \end{cases}$$

(15)

where *B* is the bulk modulus.

Model Simulations

Figure 9 shows the results of monotonic drained triaxial tests and model simulations of polymer mixed rockfill aggregates plotted in the $\eta-\varepsilon_1$ ($\eta = q/p'_{pc}$) and $\varepsilon_1-\varepsilon_v$ planes. The material parameters and state variables considered for the simulations are $G_0 = 345$, $\mu = 0.3$, $c' = 0, 70, 113$, $\varphi'_0 = 49.5°$, $\Delta\varphi'_0 = 10°$, $e_0 = 0.50$, $e_{cs0} = 0.60$, $\lambda_s = 0.025$, $k_d = 0.01$, $k_b = 0.01$, $M_{cs} = 1.68$, $h_1 = 0.07$, $h_2 = 1.0$, $R = 6.5$, and $N = 2$ for the different mix proportions. The test data are presented with an open symbol, and the model simulations are the continuous lines. There is a very good fit between simulation and experiment. The model can reasonably reflect the strength and deformation characteristics of the polymer rockfill and the influence of the polymer content. With the polymer content increase, the strength of the polymer rockfill increases, and the dilatancy increases.

Conclusions

In this paper, a combined laboratory and constitutive modeling approaches were adopted to evaluate the triaxial response of rockfill aggregates mixed with a polymer. The stress–strain and volume change behavior of polymeric rockfill at different polymer contents of 0 %, 2 % and 4 % were observed. The results revealed that the strength and deformation characteristics of the polymer blended rockfill aggregates are substantially different from those of the conventional coarse aggregates without the use of the polymer. When the content of the polymer increases, the strength increases, and the deformation decreases. The critical stress ratio of polymer aggregates mix is less affected by the polymer content, and the critical stress ratios of different polymer contents are equal when cohesion of polymer is considered as additional average effective stress.

    The polymer can be considered as voids or solids during the analysis. When the polymer is considered as solids, the critical state line in $e-(p'_{pc}/p_a)^{0.7}$ of different polymer rockfills is basically the same; when the polymer is considered as voids, the critical state lines are approximately parallel to each other. The relationships of critical stress ratio and critical state line are based on the limited test data and need further validation for a wider range of particle sizes and polymer contents.

    A new boundary surface model to capture the effect of polymer additive on the rockfill aggregates is proposed. In this model, the effect of polymer content is considered as additional average effective stress. A state parameter considering pressure and void ratio is used. The boundary surface is a teardrop shape, which is similar to the University of New South Wales (UNSW) model[38] bounding surface model. The model requires 15 model parameters (G_0, μ, c', φ'_0, $\Delta\varphi'_0$, e_0, e_{cs0}, λ_s, k_d, k_b, M_{cs}, h_1, h_2, R and N). The model captures the characteristic features of the polymer rockfill aggregates for particle breakage (φ'_0 and $\Delta\varphi'_0$) and polymer content (c'). The results of the simulations were invariably in excellent agreement with the triaxial test, which indicates the capability of the model in reproducing the strength and deformation of rockfill aggregates mixed with polymer.

References

1.   B. Chandrasekaran, B. B. Broms, and K. S. Wong, "Strength of Fabric Reinforced Sand under Axisymmetric Loading," *Geotextiles and Geomembranes* 8, no. 4 (1989): 293–310, https://doi.org/10.1016/0266-1144(89)90013-7
2.   W. Cui and M. Xiao, "Centrifuge Modeling of Geogrid-Reinforced and Rammed Soil-Cement Column-Supported Embankment on Soft Soil," *Journal of Testing and Evaluation* 48, no. 5 (September 2020): 4016–4029, https://doi.org/10.1520/JTE20170603
3.   Y. S. Hong and C. S. Wu, "The Performance of a Sand Column Internally Reinforced with Horizontal Reinforcement Layers," *Geotextiles and Geomembranes* 41 (2013): 36–49, https://doi.org/10.1016/j.geotexmem.2013.10.002
4.   J. Lai and B. H. Yang, "Laboratory Testing and Numerical Simulation of a Strip Footing on Geosynthetically Reinforced Loose Sand," *Journal of Testing and Evaluation* 45, no. 1 (January 2017): 51–60, https://doi.org/10.1520/JTE20160444

5. B. J. Nareeman and M. Y. Fattah, "Effect of Soil Reinforcement on Shear Strength and Settlement of Cohesive-Frictional Soil," *International Journal of GEOMATE* 3, no. 1 (2012): 308–313.

6. M. Y. Fattah, M. R. Mahmood, and M. F. Aswad, "Experimental and Numerical Behavior of Railway Track Over Geogrid Reinforced Ballast Underlain by Soft Clay," in *First GeoMEast International Congress and Exhibition* (Cham, Switzerland: Springer, 2018).

7. F. Ahmad, F. Bateni, and M. Azmi, "Performance Evaluation of Silty Sand Reinforced with Fibres," *Geotextiles and Geomembranes* 28, no. 1 (February 2010): 93–99, https://doi.org/10.1016/j.geotexmem.2009.09.017

8. R. H. Chen, Y. W. Huang, and F. C. Huang, "Confinement Effect of Geocells on Sand Samples under Triaxial Compression," *Geotextiles and Geomembranes* 37 (April 2013): 35–44, https://doi.org/10.1016/j.geotexmem.2013.01.004

9. A. Hamidi and M. Hooresfand, "Effect of Fiber Reinforcement on Triaxial Shear Behavior of Cement Treated Sand," *Geotextiles and Geomembranes* 36 (2013): 1–9, https://doi.org/10.1016/j.geotexmem.2012.10.005

10. O. Plé and T. N. H. Lê, "Effect of Polypropylene Fiber-Reinforcement on the Mechanical Behavior of Silty Clay," *Geotextiles and Geomembranes* 32 (2012): 111–116, https://doi.org/10.1016/j.geotexmem.2011.11.004

11. R. Sahu, R. Ayothiraman, and G. V. Ramana, "Effect of Waste Human Hair Fibers on Shear Behavior of Sand in Dry and Saturated Conditions," *Journal of Testing and Evaluation* 47, no. 1 (July 2018): 153–173, https://doi.org/10.1520/JTE20170648

12. M. S. Chauhan, S. Mittal, and B. Mohanty, "Performance Evaluation of Silty Sand Subgrade Reinforced with Fly Ash and Fibre," *Geotextiles and Geomembranes* 26, no. 5 (October 2008): 429–435, https://doi.org/10.1016/j.geotexmem.2008.02.001

13. A. V. da Fonseca, M. F. Amaral, F. Panico, and S. Rios, "Indexation of Dynamic and Static Geomechanical Properties of a Cemented Aggregate for Transportation Engineering," *Transportation Geotechnics* 1, no. 1 (March 2014): 31–44, https://doi.org/10.1016/j.trgeo.2014.02.001

14. A. J. Alrubaye, M. Hasan, and M. Y. Fattah, "Effects of Using Silica Fume and Lime in the Treatment of Kaolin Soft Clay," *Geomechanics and Engineering* 14, no. 3 (2018): 247–255.

15. M. Y. Fattah, F. H. Rahil, and K. Y. H. Al-Soudany, "Improvement of Clayey Soil Characteristics Using Rice Husk Ash," *Journal of Civil Engineering and Urbanism* 3, no. 1 (February 2013): 12–18.

16. A. J. Alrubaye, M. Hasan, and M. Y. Fattah, "Improving Geotechnical Characteristics of Kaolin Soil Using Silica Fume and Lime," *Special Topic & Reviews in Porous Media: An International Journal* 7, no. 1 (2016): 77–85, https://doi.org/10.1615/SpecialTopicsRevPorousMedia.v7.i1.70

17. N. C. Consoli, D. Foppa, L. Festugato, and K. S. Heineck, "Key Parameters for Strength Control of Artificially Cemented Soils," *Journal of Geotechnical and Geoenvironmental Engineering* 133, no. 2 (2007): 197–205, https://doi.org/10.1061/(ASCE)1090-0241(2007)133:2(197)

18. J. Liu, F. H. Liu, X. J. Kong, and L. Yu, "Large-Scale Shaking Table Model Tests on Seismically Induced Failure of Concrete-Faced Rockfill Dams," *Soil Dynamics and Earthquake Engineering* 82 (March 2016): 11–23, https://doi.org/10.1016/j.soildyn.2015.11.009

19. G. Yang, T. Yu, X. Yang, and B. Han, "Seismic Resistant Effects of Composite Reinforcement on Rockfill Dams Based on Shaking Table Tests," *Journal of Earthquake Engineering* 21, no. 6 (2017): 1010–1022, https://doi.org/10.1080/13632469.2016.1190800

20. X. Zhou, G. Ma, and Y. D. Zhang, "Grain Size and Time Effect on the Deformation of Rockfill Dams: A Case Study on the Shuibuya CFRD," *Géotechnique* 69, no. 7 (July 2019): 606–619, https://doi.org/10.1680/jgeot.17.P.299

21. A. K. Gupta, "Effects of Particle Size and Confining Pressure on Breakage Factor of Rockfill Materials Using Medium Triaxial Test," *Journal of Rock Mechanics and Geotechnical Engineering* 8, no. 3 (June 2016): 378–388, https://doi.org/10.1016/j.jrmge.2015.12.005

22. E. Frossard, W. Hu, C. Dano, and P. Y. Hicher, "Rockfill Shear Strength Evaluation: A Rational Method Based on Size Effects," *Géotechnique* 62, no. 5 (May 2012): 415–427, https://doi.org/10.1680/geot.10.P.079

23. Y. Xiao, M. Q. Meng, A. Daouadji, Q. S. Chen, Z. J. Wu, and X. Jiang, "Effects of Particle Size on Crushing and Deformation Behaviors of Rockfill Materials," *Geoscience Frontiers* 11, no. 2 (March 2020): 375–388, https://doi.org/10.1016/j.gsf.2018.10.010

24. A. Keene, J. Tinjum, and T. B. Edil, "Mechical Properties of Polymerthane Stabilized-Ballast," *Geotechnical Engineering Journal of the SEAGS & AGSSEA* 45, no. 1 (2014): 67–73.

25. A. Keene, T. Edil, D. Fratta, and J. Tinjum, "Modeling the Effect of Polyurethane Stabilization on Rail Track Response," in *Geo-Congress 2013* (Reston, VA: American Society of Civil Engineers, 2013), 1410–1419.

26. W. X. Dong, L. M. Hu, Y. Z. Yu, and H. Lv, "Comparison between Duncan and Chang's EB Model and the Generalized Plasticity Model in the Analysis of a High Earth-Rockfill Dam," *Journal of Applied Mathemathics* 2013 (2013): 709430.

27. M. Pastor, O. C. Zienkiewicz, and A. H. C. Chan, "Generalized Plasticity and the Modelling of Soil Behaviour," *International Journal for Numerical and Analyitical Methods in Geomechanics* 14, no. 3 (April 1990): 151–190, https://doi.org/10.1002/nag.1610140302

28. C. S. Desai, *Mechanics of Materials and Interfaces: The Disturbed State Concept* (Boca Raton, FL: CRC Press, 2001).

29. A. Varadarajan, K. G. Sharma, K. Venkatachalam, and A. K. Gupta, "Testing and Modeling Two Rockfill Materials," *Journal of Geotechnical and Geoenvironmental Engineering* 129, no. 3 (March 2003): 206–218, https://doi.org/10.1061/(ASCE)1090-0241(2003)129:3(206)

30. Y. Xiao and H. L. Liu, "Elastoplastic Constitutive Model for Rockfill Materials Considering Particle Breakage," *International Journal of Geomechanics* 17, no. 1 (January 2017): 04016041, https://doi.org/10.1061/(ASCE)GM.1943-5622.0000681

31. M. E. Kan, H. A. Taiebat, and N. Khalili, "Simplified Mapping Rule for Bounding Surface Simulation of Complex Loading Paths in Granular Materials," *International Journal of Geomechanics* 14, no. 2 (April 2014): 239–253, https://doi.org/10.1061/(ASCE)GM.1943-5622.0000307

32. Y. Xiao, H. L. Liu, Y. M. Chen, and J. S. Jiang, "Bounding Surface Model for Rockfill Materials Dependent on Density and Pressure under Triaxial Stress Conditions," *Journal of Engineering Mechanics* 140, no. 4 (April 2014): 04014002, https://doi.org/10.1061/(ASCE)EM.1943-7889.0000702

33. M. E. Kan and H. A. Taiebat, "Application of Advanced Bounding Surface Plasticity Model in Static and Seismic Analyses of Zipingpu Dam," *Canadian Geotechnical Journal* 53, no. 3 (2016): 455–471, https://doi.org/10.1139/cgj-2015-0120

34. Y. Vasistha, A. K. Gupta, and V. Kanwar, "Prediction of Shear Strength Parameters of Two Rockfill Materials," *Electronic Journal of Geotechnical Engineering* 17 (2012): 3221–3232.

35. X. S. Li and Y. Wang, "Linear Representation of Steady-State Line for Sand," *Journal of Geotechnical and Geoenvironmental Engineering* 124, no. 12 (December 1998): 1215–1217, https://doi.org/10.1061/(ASCE)1090-0241(1998)124:12(1215)

36. R. G. Wan and P. J. Guo, "A Simple Constitutive Model for Granular Soils: Modified Stress-Dilatancy Approach," *Computers and Geotechnics* 22, no. 2 (1998): 109–133, https://doi.org/10.1016/S0266-352X(98)00004-4

37. Z. L. Wang, Y. F. Dafalias, X. S. Li, and F. I. Makdisi, "State Pressure Index for Modeling Sand Behavior," *Journal of Geotechnical and Geoenvironmental Engineering* 128, no. 6 (June 2002): 511–519, https://doi.org/10.1061/(ASCE)1090-0241(2002)128:6(511)

38. N. Khalili, M. A. Habte, and S. Valliappan, "A Bounding Surface Plasticity Model for Cyclic Loading of Granular Soils," *International Journal for Numerical Methods in Engineering* 63, no. 14 (August 2005): 1939–1960, https://doi.org/10.1002/nme.1351

39. Y. Xiao, H. L. Liu, Y. M. Chen, J. S. Jiang, and W. G. Zhang, "Testing and Modeling of the State-Dependent Behaviors of Rockfill Material," *Computers and Geotechnics* 61 (September 2014): 153–165, https://doi.org/10.1016/j.compgeo.2014.05.009